Energy Storage Controller Synthesis for Power Systems With Temporal Logic Specifications

Zhe Xu, *Student Member, IEEE*, Agung Julius, *Member, IEEE*, and Joe H. Chow, *Fellow, IEEE*

***Abstract*—We present an energy storage controller synthesis method for power systems with respect to metric temporal logic (MTL) specifications. The power systems with both constant impedance loads and constant power loads are modeled as a set of differential–algebraic equations. After a fault is cleared, with uncertainties in the fault clearing time, the generator machine angles and rotor speed deviations will enter a set of postfault initial states. We use the robust neighborhood approach to cover this set using the initial robust neighborhoods of finitely many simulated postfault trajectories. These simulated postfault trajectories meet the frequency regulation requirements specified in MTL as they are driven by the optimal control input signals obtained through a functional gradient descent approach. In this way, all the possible postfault trajectories with the given uncertainties in the fault clearing time are guaranteed to satisfy the MTL specification. Furthermore, we learn a piecewise linear control law from the data of the simulated trajectories to generate a feedback controller.**

***Index Terms*—Controller synthesis, differential–algebraic equations, energy storage systems (ESSs), temporal logic.**

I. Introduction

In RECENT years, power systems are increasingly utilizing diversified power resources for providing more reliable and efficient ancillary services [1], [2]. The market-based mechanism has provided incentives for improving the performance of various ancillary services. Unlike the traditional ancillary services, market with no differentiation for resources that can respond more quickly or accurately, current and future ancillary services markets are increasingly focusing on the performance of different resources [3]. With the incorporation of renewable energy in the ancillary services, energy storage systems (ESSs) such as flywheels, supercapacitors, and battery ESSs serve as buffers of the power system to restore grid frequency to the allowable range [4]. The ESSs perform better than traditional generators and operating reserves with their quicker responsive capability, more precise control and capability to store and release energy in providing nearly net-zero energy services [5], [6].

As different ancillary services and ESSs have different response time and duration time, the regulated frequency could have different temporal properties. Therefore, temporal logic [7], [8] can be utilized to provide time-related specifications such as "after a fault is cleared, the grid frequency should be restored to 60 Hz $\pm$ 0.2 Hz within 2 s and to 60 Hz $\pm$ 0.02 Hz within 20 s." The ESSs that can meet frequency and stability requirement in the form of temporal logic specifications have more precise time-related performance measure, which can create potential economic benefits in the performance-based ancillary services market. There are a lot of literature on the control of ESSs for economic and stability benefits, while incorporating temporal logic constraints into the controller synthesis problem is still a novel approach.

A. Related Works

In the literature, there are two main categories of approaches of designing controllers that meet certain temporal logic specifications. The first category of approaches abstract the system as a transition system and transform the controller synthesis problem into a series of constrained reachability problems [9]–[11]. This category of approaches have been mostly used in controller synthesis with respect to discrete-time temporal logics such as linear temporal logic (LTL). The second category of approaches convert the controller synthesis problem into a single optimal control problem and encode the temporal logic specifications as optimization constraints on the optimization variables. These category of approaches are mainly used in continuous-time (real-time, dense-time) temporal logics such as metric temporal logic (MTL) and signal temporal logic. For the optimization problem formulation, some authors formulate it as a mixed-integer linear programming problem for mixed logical dynamical systems [12], [13] while some other authors substitute the temporal logic constraint into the optimization objectives and apply a functional gradient descent algorithm on the resulting unconstrained problem. The functional gradient descent approach has wider applications as it can be applied for any general nonlinear systems. In [14], Winn and Julius propose an optimal safety controller synthesis method for continuous nonlinear systems using functional gradient descent. In [15], Abbas *et al.* apply the method in the falsification of MTL specifications and the controller synthesis can be achieved by falsifying the negation of the MTL specifications.

While these methods are effective in applications such as controlling quadrotors or insulin levels in the blood with the systems modeled as a set of differential equations, they are still insufficient for power system applications as power systems are often modeled as a set of nonlinear differential–algebraic equations (nonlinear DAE systems) [16], especially when constant power

Manuscript received June 10, 2017; accepted September 23, 2017. This work was supported by the National Science Foundation under Grant CNS-1218109, Grant CNS-1550029, and Grant CNS-1618369. The material in this paper was presented at American Control Conference, Seattle, WA, USA, May 24–26, 2017. *(Corresponding author: Zhe Xu.)*

The authors are with the Department of Electrical, Computer, and Systems Engineering, Rensselaer Polytechnic Institute, Troy, NY 12180 USA (e-mail: xuz8@rpi.edu; juliua2@rpi.edu; chowj@rpi.edu).

Digital Object Identifier 10.1109/JSYST.2017.2758358

loads exist in the network [17], [18]. There has been only a few studies in controller synthesis for nonlinear DAE systems with discrete-time or continuous-time temporal logic specifications such as [19] where the authors designed a hybrid controller for switched DAE systems with LTL specifications. There has been literature in the reachability analysis of power systems modeled as DAE systems [20], but it has not been applied to controller synthesis of such systems.

B. Contributions and Advantages

1) Feedforward Controller Synthesis for the Power System Nonlinear DAE Model with Uncertainties in the Initial State with respect to MTL Specifications: We present a controller synthesis method to regulate grid frequencies utilizing ESSs and we seek the minimal-storage-effort control to satisfy certain MTL specifications of the frequency deviations and machine angles. Our method is based on the functional gradient descent method in [15], but different from [15], we formulate the MTL specification as a constraint and we apply the functional gradient descent method to both satisfy the MTL constraint and minimize an objective function as a performance metric of the controller. A preliminary version of this paper appeared in conference proceedings [21], where we present the energy controller synthesis of power systems modeled as a set of differential equations. In this paper, the gradients of both the objective and the constraint functions are calculated specifically for DAE systems. While our methodology is applicable for general nonlinear DAE systems, as the power system DAE model is feedback linearizable, we choose to utilize that for the purpose of easier computation (less computation time) and the obtained feedback linearized system has a control autobisimulation function, which can bound the divergence of trajectories that start from an initial set within the robust neighborhood [22]. We simulate finitely many postfault trajectories (after the fault is cleared) with different fault clearing time such that the initial robust neighborhoods of these simulated trajectories can cover all the postfault initial states (all the possible states when the fault is cleared) with given uncertainties in the fault clearing time. For each simulated postfault trajectory, the optimal storage control input signals are computed through the functional gradient descent method. In this way, all the postfault trajectories that start from the set of postfault initial states (including the uncertainties in the fault clearing time) are guaranteed to stay in the robust neighborhoods around the nominal (simulated) trajectories and satisfy the MTL specifications.

2) Feedback Controller Synthesis with Respect to MTL Specifications: In [23], Winn and Julius replace the feedforward controller obtained in [14] with a feedback controller and a piecewise linear control law is learned from the data of the simulated trajectories following the approach of Bemporad *et al.* [24]. Following this path, we generate a feedback controller by identifying a piecewise linear control law from the data of the optimal input signals and the states of the simulated trajectories, but different from [23], we generate a feedback controller for MTL specifications, which requires more stringent conditions than that for safety specifications in [23]. Another difference from other works such as [23] is that we use robust linear programming (LP) to find the classification functions for the subclasses and construct piecewise linear classifiers in partitioning the state space so that the state space is totally covered. We have proven and tested with simulations that any trajectory starting from the initial set with the feedback controller are guaranteed to satisfy the MTL specification. Besides, simulations show that even when unexpected disturbances occur, trajectories generated with the feedback controller can still satisfy the MTL specification in certain cases and have better performance in comparison with the trajectories generated with the feedforward controller.

This paper is structured as follows. Section II briefly reviews the MTL and the control autobisimulation function. Section III shows the controller synthesis methods for both the feedforward and feedback controllers with nonlinear DAE systems and MTL specifications. Section IV shows the implementation of the algorithms on a double-machine infinite-bus power system model to control the ESSs with MTL specifications. Finally, some conclusions are presented in Section V.

II. Preliminaries

A. Metric Temporal Logic

In this section, we briefly review the MTL that are interpreted over continuous-time signals [25], the MTL interpreted over discrete-time signals can be found in [26]. The state of the system we are studying is described by a set of n variables that can be written as a vector $x = [x_1, x_2, \ldots, x_n]^T$. The domain of x is denoted by $\mathbb{X} = \mathbb{X}_1 \times \mathbb{X}_2 \times \cdots \times \mathbb{X}_n$ ($\mathbb{X}_i$ is a subset of $\mathbb{R}$). The domain $\mathbb{B} = \{true, false\}$ is the Boolean domain and the time set is $\mathbb{T} = \mathbb{R}_{\geqslant 0}$. A trajectory (or signal) s describing an evolution of the system is a function from $\mathbb{T}$ to $\mathbb{X}$. A set AP is a set of atomic propositions, each mapping $\mathbb{X}$ to $\mathbb{B}$. The syntax of MTL is defined recursively as follows:

$$\phi := \top \mid \pi \mid \neg\phi \mid \phi_1 \wedge \phi_2 \mid \phi_1 \vee \phi_2 \mid \phi_1 \mathcal{U}_{\mathcal{I}} \phi_2$$

where $\top$ stands for the Boolean constant True, $\pi \in AP$ is an atomic proposition, $\neg$ (negation), $\wedge$(conjunction), $\vee$ (disjunction) are standard Boolean connectives, $\mathcal{U}$ is a temporal operator representing "until," $\mathcal{I}$ is a time interval of the form $\mathcal{I} = [i_1, i_2)$. We can also derive two useful temporal operators from "until" ($\mathcal{U}$), which are "eventually" $\Diamond_{\mathcal{I}}\phi = \top \mathcal{U}_{\mathcal{I}} \phi$ and "always" $\Box_{\mathcal{I}}\phi = \neg\Diamond_{\mathcal{I}}\neg\phi$. We define the set of states that satisfy the atomic proposition π as $\mathcal{O}(\pi) \in \mathbb{X}$. We denote $\langle\langle\phi\rangle\rangle(s,\tau) = \top$ if the state of the trajectory s satisfies the formula ϕ at time τ. Then, the Boolean semantics of MTL are defined recursively as follows [25]:

$$\begin{aligned}
\langle\langle\top\rangle\rangle(s,\tau) &:= \top \\
\langle\langle\pi\rangle\rangle(s,\tau) &:= s(\tau) \in \mathcal{O}(\pi) \\
\langle\langle\neg\phi\rangle\rangle(s,\tau) &:= \neg\langle\langle\phi\rangle\rangle(s,\tau) \\
\langle\langle\phi_1 \vee \phi_2\rangle\rangle(s,\tau) &:= \langle\langle\phi_1\rangle\rangle(s,\tau) \vee \langle\langle\phi_2\rangle\rangle(s,\tau) \\
\langle\langle\phi_1 \mathcal{U}_{\mathcal{I}} \phi_2\rangle\rangle(s,\tau) &:= \bigvee_{\tau' \in (\tau + \mathcal{I})} \Big(\langle\langle\phi_2\rangle\rangle(s,\tau') \wedge \bigwedge_{\tau \leq \tau'' < \tau'} \langle\langle\phi_1\rangle\rangle \\
&\qquad (s,\tau'') \Big)
\end{aligned}$$

where $\tau + \mathcal{I} = \{\tau + \tilde{\tau} | \tilde{\tau} \in \mathcal{I}\}$.

We denote the distance from x to a set $S \subseteq \mathbb{X}$ as $\mathbf{dist}_d(x, S) \triangleq \inf\{d(x,y) | y \in cl(S)\}$ where d is a metric on $\mathbb{X}$ and $cl(S)$

denotes the closure of the set S. In this paper, we use the metric $d(x,y)=\|x-y\|$, where $\|\cdot\|$ denotes the 2-norm. We denote the depth of x in S as $\mathbf{depth}_d(x,S) \triangleq \mathbf{dist}_d(x,\mathbb{X}\setminus S)$, the signed distance from x to S as

$$\mathbf{Dist}_d(x,S) \triangleq \begin{cases} -\mathbf{dist}_d(x,S), & \text{if } x\notin S \\ \mathbf{depth}_d(x,S), & \text{if } x\in S. \end{cases} \tag{1}$$

We use $[[\phi]](s,\tau)$ to denote the robustness degree of the trajectory s with respect to the formula ϕ at time τ. The robust semantics of a formula ϕ with respect to s are defined recursively as follows [25]:

$$\begin{aligned}
[[\top]](s,\tau) &:= +\infty \\
[[\pi]](s,\tau) &:= \mathbf{Dist}_d(s(\tau),\mathcal{O}(\pi)) \\
[[\neg\phi]](s,\tau) &:= -[[\phi]](s,\tau) \\
[[\phi_1 \vee \phi_2]](s,\tau) &:= \max\big([[\phi_1]](s,\tau),[[\phi_2]](s,\tau)\big) \\
[[\phi_1 \mathcal{U}_{\mathcal{I}} \phi_2]](s,\tau) &:= \max_{\tau'\in(\tau+\mathcal{I})}\Big(\min\big([[\phi_2]](s,\tau'), \\
&\qquad \min_{\tau\le\tau''<\tau'}[[\phi_1]](s,\tau'')\big)\Big).
\end{aligned}$$

As an example, the trajectory $s(\tau)=\sin(\tau)$ $(\tau\in[0,+\infty))$ satisfies the formula $\square_{[\pi/6,\pi/2)}(x>0)$ (which reads as "During the time interval of $[\pi/6,\pi/2)$, $s(\tau)$ is always greater than 0") at time 0 with robustness degree $[[\phi]](s,0)=0.5$.

B. Control Autobisimulation Function

Consider a nonlinear DAE system with input

$$\begin{aligned}
\dot{x} &= f(x,z)+\sum_{i=1}^{p} g_i(x,z)u_i \\
0 &= \sigma(x,z)
\end{aligned} \tag{2}$$

where the state $x=[x_1,x_2,\ldots,x_n]^T\in\mathbb{R}^n$, $z=[z_1,z_2,\ldots,z_m]^T\in\mathbb{R}^m$, the input $u=[u_1,u_2,\ldots,u_p]^T\in\mathbb{R}^p$, $f:\mathbb{R}^n\times\mathbb{R}^m\to\mathbb{R}^n$, $g_i:\mathbb{R}^n\times\mathbb{R}^m\to\mathbb{R}^n (i=1,\ldots,p)$, and $\sigma:\mathbb{R}^n\times\mathbb{R}^m\to\mathbb{R}^m$ are smooth vector fields.

If we define the constraint manifold as $\Xi=\{(x,z)|\sigma(x,z)=0\}$, then the singular manifold is defined as $\Upsilon=\{(x,z)\in\Xi|\det\frac{\partial\sigma(x,z)}{\partial z}=0\}$.

Assumption 1: In the following, we assume that the trajectories of the system described by (2) do not enter the singular manifold, i.e., $\mathrm{rank}(\frac{\partial\sigma(x,z)}{\partial z})=m$ always holds.

According to [27] and [28], we have the following definition:

Definition 1: For the system described by (2), let $h_i:\mathbb{R}^n\times\mathbb{R}^m\to\mathbb{R}(i=1,\ldots,p)$ be smooth output functions. The M derivative of h_i along f is a function $\mathbb{R}^n\times\mathbb{R}^m\to\mathbb{R}$, denoted as $M_f h_i(x,z)$ and defined as $M_f h_i(x,z)$

$$= \left(\frac{\partial h_i(x,z)}{\partial x}-\frac{\partial h_i(x,z)}{\partial z}\left(\frac{\partial\sigma(x,z)}{\partial z}\right)^{-1}\frac{\partial\sigma(x,z)}{\partial x}\right) f(x,z). \tag{3}$$

If h_i is differentiated k times along f, the function $M_f^k h_i$ can be defined as $M_f^k h_i = M_f(M_f^{k-1}h_i)$ with $M_f^0 h_i = h_i$.

If the system described by (2) is state feedback linearizable using the M derivative [28], we can introduce a new control input $\rho\in\mathbb{R}^p$, choose output functions $h_i(x,z)(i=1,\ldots,p)$ and design a feedback law as $u=\kappa(x,z)+\lambda(x,z)\rho$, where

$$\begin{aligned}
\lambda(x,z) &= \varrho(x,z)^{-1} \\
&= \begin{bmatrix} M_{g_1}M_f^{r_1-1}h_1(x,z) & \ldots & M_{g_p}M_f^{r_1-1}h_1(x,z) \\ M_{g_1}M_f^{r_2-1}h_2(x,z) & \ldots & M_{g_p}M_f^{r_2-1}h_2(x,z) \\ \ldots & \ldots & \ldots \\ M_{g_1}M_f^{r_p-1}h_p(x,z) & \ldots & M_{g_p}M_f^{r_p-1}h_p(x,z) \end{bmatrix}^{-1} \\
\kappa(x,z) &= -\lambda(x,z)\cdot[M_f^{r_1}h_1(x,z),\ldots,M_f^{r_p}h_p(x,z)]^T
\end{aligned} \tag{4}$$

where $r=[r_1,\ldots,r_p]$ is the vector relative degree, i.e., $r_i=\min\{k|M_{g_j}M_f^{k-1}h_i(x,z)\neq 0 \text{ for at least one } j\}$ and $\det(\varrho(x,z))\neq 0$, $r_1+r_2+\cdots+r_p=n$. In this way, the closed-loop system with the new input ρ is a linear system, as shown in Fig. 2.

We denote the feedback linearized system dynamics as follows:

$$\dot{\eta}=A\eta+B\rho \tag{5}$$

where $\eta\in\mathbb{R}^n$ is the new state of the feedback linearized system, which can be expressed as a function of x and z:

$$\eta(x,z)=\begin{bmatrix} h_1(x,z) \\ \ldots \\ M_f^{r_1-1}h_1(x,z) \\ \ldots \\ \ldots \\ h_p(x,z) \\ \ldots \\ M_f^{r_p-1}h_p(x,z) \end{bmatrix}. \tag{6}$$

When the state is not in the singular manifold Υ, according to the implicit function theorem, z can be represented as a function of x. Thus, it can be proven that there exists a diffeomorphism $\eta=T(x)$ [29], therefore both x and z can be represented as a function of η. For the system described by (5), a control autobisimulation function can be formed [22].

Definition 2: A continuously differentiable function $\psi:\mathbb{R}^n\times\mathbb{R}^n\to\mathbb{R}_+$ is a control autobisimulation function of the system described by (5) if for any $\eta,\eta'\in\mathbb{R}^n$, $\psi(\eta,\eta')\ge\|\eta-\eta'\|$, and there exists a function $\rho:\mathbb{R}^n\to\mathbb{R}^p$ such that

$$\nabla_\eta\psi(\eta,\eta')(A\eta+B\rho(\eta))+\nabla_{\eta'}\psi(\eta,\eta')(A\eta'+B\rho(\eta'))\le 0. \tag{7}$$

Following [22], we can introduce another input v such that $\rho(\eta)=K\eta+v$, where $K\in\mathbb{R}^{p\times n}$ is chosen such that $A+BK$ is Hurwitz (this is referred to as stabilization). In this way, a control autobisimulation function can be formed as follows:

$$\psi(\eta,\eta')=[(\eta-\eta')^T P(\eta-\eta')]^{\frac{1}{2}} \tag{8}$$

where P and K satisfy

$$\begin{aligned}
P^T &= P\succeq 0 \\
(A+BK)^T P+P(A+BK) &\preceq 0.
\end{aligned} \tag{9}$$

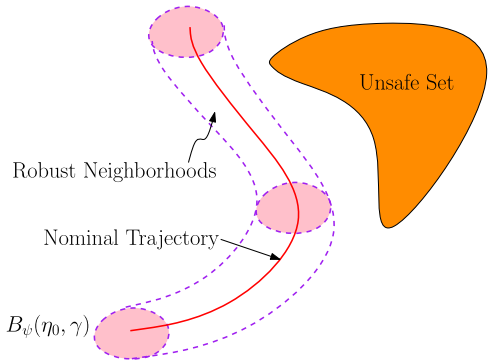

Fig. 1. Trajectories that start from the initial robust neighborhood (robustness ellipsoid) $B_\psi(\eta_0,\gamma)$ are guaranteed to stay in the robust neighborhoods around the nominal (simulated) trajectory and satisfy the MTL specification ϕ (such as not entering the unsafe set for a certain period of time).

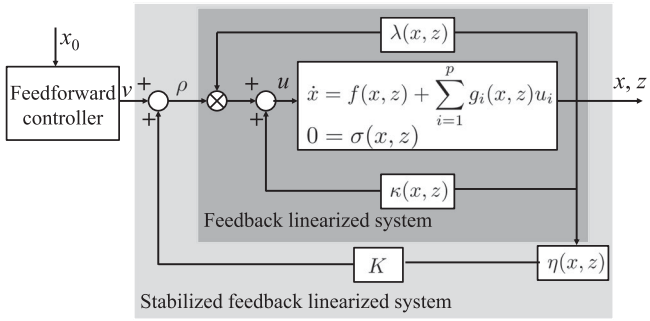

Fig. 2. Diagram of the feedforward controller with the stabilized feedback linearized system.

For brevity, we denote $F(\eta,v) \triangleq (A+BK)\eta + Bv$. We denote the solution of the stabilized feedback linearized system $\dot{\eta} = F(\eta,v)$ as $\xi(\tau;\eta_0,v)$, where η_0 is the initial state of the feedback linearized system. We denote $B_\psi(\eta,\gamma) \triangleq \{\eta' | \psi(\eta,\eta') \leq \gamma\}$ as the robust neighborhood of a point η in the shape of an ellipsoid (robustness ellipsoid) and γ is referred to as the radius of the ellipsoid. As the control autobisimulation function is nonincreasing through time, it is guaranteed that for any initial state $\eta_0' \in \mathbb{R}^n$ and any input signal $v(\tau)$, if the initial distance $\psi(\eta_0,\eta_0') = \gamma$, then for any time τ, $\xi(\tau;\eta_0',v) \in B_\psi(\xi(\tau;\eta_0,v),\gamma)$ (as shown in Fig. 1).

III. Controller Synthesis

A. Feedforward Controller Synthesis

As discussed in Section II-B, both x and z can be represented as a function of $\xi(\tau;\eta_0,v)$ when the state is not in the singular manifold Υ. The core of the feedforward controller synthesis problem that we consider in this paper is to find the input v such that the trajectory $x(\xi(\cdot;\eta_0,v))$ satisfies the MTL specification ϕ with minimal control efforts for the original input u. As shown in Fig. 2, although there are feedback innerloops for the feedback linearization and stabilization, it is a feedforward controller for the stabilized feedback linearized system. The optimization problem is formulated as follows:

$$\begin{aligned} \text{min.} \quad & \int_0^T g(\xi(\tau;\eta_0,v),v(\tau))d\tau \\ \text{s.t.} \quad & [[\phi]](x(\xi(\cdot;\eta_0,v)),0) \geq \zeta \end{aligned} \tag{10}$$

where ζ is a positive number to avoid too small robustness ellipsoid and $g(\xi(\tau;\eta_0,v),v(\tau))$ can be expressed as follows:

$$\begin{aligned} & g(\xi(\tau;\eta_0,v),v(\tau)) \\ & = \|u(\tau)\|^2 \\ & = ||\kappa\big(x(\xi(\tau;\eta_0,v)),z(\xi(\tau;\eta_0,v))\big) \\ & \quad + \lambda\big(x(\xi(\tau;\eta_0,v)),z(\xi(\tau;\eta_0,v))\big)\big(K\xi(\tau;\eta_0,v)+v(\tau)\big)||^2. \end{aligned}$$

We can use functional gradient descent method to decrease $[[\neg\phi]](x(\xi(\cdot;\eta_0,v)),0)$, which is equivalent to increasing $[[\phi]](x(\xi(\cdot;\eta_0,v)),0)$, at each iteration step until the constraint is satisfied. As $F(\eta,v)$ is linear with respect to η and v, the solution $\xi(\tau;\eta_0,v)$ is unique and absolutely continuous, the flow F is locally bounded. According to [30, Proposition 3.1], for the MTL formula $\neg\phi$, there exists a critical time $\tau_{\text{r}} \in [0,T]$ and a critical proposition $\pi_{\text{r}} \in AP$ (see Section II-A) such that $[[\neg\phi]](x(\xi(\cdot;\eta_0,v)),0) = \mathbf{Dist}_d(x(\xi(\tau_{\text{r}};\eta_0,v)),\mathcal{O}(\pi_{\text{r}}))$. Thus, the robustness degree of the trajectory $x(\xi(\cdot;\eta_0,v))$ with respect to $\neg\phi$ can be calculated by identifying the critical time τ_{r} and the critical proposition π_{r} (which can be easily computed using software such as S-TaLiRo [31]).

Thus, at each iteration the optimization problem is converted to the following problem:

$$\begin{aligned} \text{min.} \quad & \int_0^T g(\xi(\tau;\eta_0,v),v(\tau))d\tau \\ \text{s.t.} \quad & G(\xi(\tau_{\text{r}};\eta_0,v)) + \zeta \leq 0 \end{aligned} \tag{11}$$

where $G(\xi(\tau_{\text{r}};\eta_0,v)) = [[\neg\phi]](x(\xi(\cdot;\eta_0,v)),0) = \mathbf{Dist}_d(x(\xi(\tau_{\text{r}};\eta_0,v)),\mathcal{O}(\pi_{\text{r}}))$. For brevity, we denote $J(v) \triangleq \int_0^T g(\xi(\tau;\eta_0,v),v(\tau))d\tau$ and $J_{\text{con}}(v) \triangleq G(\xi(\tau_{\text{r}};\eta_0,v)) + \zeta$ as the objective function and the constraint function, respectively.

We compute the functional derivative of $J(v)$ with respect to the input signal v in the direction $\hat{v}$,

$$dJ(v;\hat{v}) \triangleq \lim_{\delta\to 0} \frac{J(v+\delta\hat{v}) - J(v)}{\delta}. \tag{12}$$

If we denote $q(\cdot)$ as the gradient of J in the function space of $v(\cdot)$, then we have

$$dJ(v;\hat{v}) \triangleq \langle q,\hat{v}\rangle = \int_0^T q(\tau)\hat{v}(\tau)d\tau. \tag{13}$$

Similarly, the functional derivative of $J_{\text{con}}(v)$ with respect to v in the direction $\hat{v}_{\text{con}}$ can be written as follows:

$$\begin{aligned} dJ_{\text{con}}(v;\hat{v}_{\text{con}}) & \triangleq \lim_{\delta\to 0} \frac{J_{\text{con}}(v+\delta\hat{v}_{\text{con}}) - J_{\text{con}}(v)}{\delta} \\ & \triangleq \langle q_{\text{con}},\hat{v}_{\text{con}}\rangle \\ & = \int_0^T q_{\text{con}}(\tau)\hat{v}_{\text{con}}(\tau)d\tau \end{aligned} \tag{14}$$

where $q_{\text{con}}(\cdot)$ is the gradient of J_{con} in the function space of $v(\cdot)$.

In the following, we use the following notations for the sake of brevity:

$$\begin{aligned}
&\tilde{v} \triangleq v + \delta\hat{v}, \tilde{v}_{\text{con}} \triangleq v + \delta\hat{v}_{\text{con}}, \ \frac{\partial G(\tau_{\text{r}})}{\partial \eta} \triangleq \frac{\partial G}{\partial \eta}\mid_{\xi(\tau_{\text{r}};\eta_0,v)} \\
&F(\tau) \triangleq F(\xi(\tau;\eta_0,v),v(\tau)), \ g(\tau) \triangleq g(\xi(\tau;\eta_0,v),v(\tau)) \\
&\tilde{F}(\tau) \triangleq F(\xi(\tau;\eta_0,\tilde{v}),\tilde{v}(\tau)), \ \tilde{g}(\tau) \triangleq g(\xi(\tau;\eta_0,\tilde{v}),\tilde{v}(\tau)) \\
&\frac{\partial F(\tau)}{\partial \eta} \triangleq \frac{\partial F}{\partial \eta}\mid_{(\xi(\tau;\eta_0,v),v(\tau))}, \ \frac{\partial g(\tau)}{\partial \eta} \triangleq \frac{\partial g}{\partial \eta}\mid_{(\xi(\tau;\eta_0,v),v(\tau))} \\
&\frac{\partial F(\tau)}{\partial v} \triangleq \frac{\partial F}{\partial v}\mid_{(\xi(\tau;\eta_0,v),v(\tau))}, \ \frac{\partial g(\tau)}{\partial v} \triangleq \frac{\partial g}{\partial v}\mid_{(\xi(\tau;\eta_0,v),v(\tau))}.
\end{aligned} \tag{15}$$

We obtain the Taylor series expansion of $\tilde{g}(\tau)$ at $g(\tau)$ and $G(\xi(\tau_{\text{r}};\eta_0,\tilde{v}))$ at $G(\xi(\tau_{\text{r}};\eta_0,v))$ as follows:

$$\begin{aligned}
\tilde{g}(\tau) = g(\tau) &+ \delta\frac{\partial g(\tau)}{\partial x}\frac{dx}{d\eta}d\xi_\tau(v;\hat{v}) \\
&+ \delta\frac{\partial g(\tau)}{\partial z}\frac{dz}{d\eta}d\xi_\tau(v;\hat{v}) \\
&+ \delta\frac{\partial g(\tau)}{\partial v}\hat{v}(\tau) + o(\delta)
\end{aligned}$$

$$\begin{aligned}
G(\xi(\tau_{\text{r}};\eta_0,\tilde{v}_{\text{con}})) = G(\xi(\tau_{\text{r}};\eta_0,v)) &+ \delta\frac{\partial G(\tau_{\text{r}})}{\partial \eta}d\xi_{\tau_{\text{r}}}(v;\hat{v}_{\text{con}}) \\
&+ o(\delta)
\end{aligned} \tag{16}$$

where $d\xi_\tau(v;\hat{v})$ is the functional derivative of $\xi(\tau;\eta_0,v)$ with respect to v in the direction $\hat{v}$, $d\xi_{\tau_{\text{r}}}(v;\hat{v}_{\text{con}})$ is the functional derivative of $\xi(\tau_{\text{r}};\eta_0,v)$ with respect to v in the direction $\hat{v}_{\text{con}}$.

From $\sigma(x,z)=0$, we have

$$\frac{d\sigma(x,z)}{d\eta} = \frac{\partial\sigma(x,z)}{\partial x}\frac{dx}{d\eta} + \frac{\partial\sigma(x,z)}{\partial z}\frac{dz}{d\eta} = 0. \tag{17}$$

If the current state is not in the singular manifold Υ, i.e., $\frac{\partial\sigma(x,z)}{\partial z}$ is invertible, then we have

$$\frac{dz}{d\eta} = -\left(\frac{\partial\sigma(x,z)}{\partial z}\right)^{-1}\frac{\partial\sigma(x,z)}{\partial x}\frac{dx}{d\eta}. \tag{18}$$

By substituting (16) and (18) into (12) and (14), we have

$$\begin{aligned}
dJ(v,\hat{v}) = \int_0^T \Bigg(\Bigg(&\frac{\partial g(\tau)}{\partial x} - \frac{\partial g(\tau)}{\partial z}\left(\frac{\partial\sigma(x,z)}{\partial z}\right)^{-1} \\
&\frac{\partial\sigma(x,z)}{\partial x}\Bigg)\frac{dx}{d\eta}d\xi_\tau(v;\hat{v}) + \frac{\partial g(\tau)}{\partial v}\hat{v}(\tau)\Bigg)d\tau
\end{aligned} \tag{19}$$

$$dJ_{\text{con}}(v,\hat{v}_{\text{con}}) = \frac{\partial G(\tau_{\text{r}})}{\partial \eta}d\xi_{\tau_{\text{r}}}(v;\hat{v}_{\text{con}}). \tag{20}$$

Next, we write $d\xi_\tau(v;\hat{v})$ as a linear functional of $\hat{v}$ as follows:

$$d\xi_\tau(v;\hat{v}) = \langle p_\tau, \hat{v}\rangle = \int_0^\tau p_\tau(t)\hat{v}(t)dt \tag{21}$$

where $p_\tau(t)$ is an $\mathbb{R}^{n\times m}$-valued function which is specified to be zero if $\tau < t$.

By substituting (21) into (19) and (13), and changing the order of integration, we have

$$\begin{aligned}
q(t) = \frac{\partial g(t)}{\partial v} + \int_t^T \Bigg(&\frac{\partial g(\tau)}{\partial x} - \frac{\partial g(\tau)}{\partial z}\left(\frac{\partial\sigma(x,z)}{\partial z}\right)^{-1}\frac{\partial\sigma(x,z)}{\partial x}\Bigg) \\
&\frac{dx}{d\eta}p_\tau(t)d\tau.
\end{aligned} \tag{22}$$

Similarly, the gradient for the constraint function can be obtained as follows:

$$q_{\text{con}}(t) = \frac{\partial G(\tau_{\text{r}})}{\partial \eta}p_{\tau_{\text{r}}}(t). \tag{23}$$

The remaining terms that need to be calculated in (22) and (23) are $p_\tau(t)$ and $p_{\tau_{\text{r}}}(t)$. Observe that $d\xi_\tau(v;\hat{v})$ is the functional derivative of $\xi(\tau;\eta_0,v)$ in the direction $\hat{v}$, so we have

$$\begin{aligned}
d\xi_\tau(v;\hat{v}) &= \lim_{\delta\to 0}\frac{\xi(\tau;\eta_0,\tilde{v}) - \xi(\tau;\eta_0,v)}{\delta} \\
&= \lim_{\delta\to 0}\frac{1}{\delta}\int_0^\tau (\tilde{F}(s) - F(s))ds.
\end{aligned} \tag{24}$$

The Taylor series expansion of $\tilde{F}(s)$ at $F(s)$ is as follows:

$$\tilde{F}(s) = F(s) + \frac{\partial F(s)}{\partial \eta}d\xi_s(v;\hat{v})\delta + \frac{\partial F(s)}{\partial v}\hat{v}(s)\delta + o(\delta). \tag{25}$$

By substituting (25) into (24), we have

$$d\xi_\tau(v;\hat{v}) = \int_0^\tau \left(\frac{\partial F(s)}{\partial \eta}d\xi_s(v;\hat{v}) + \frac{\partial F(s)}{\partial v}\hat{v}(s)\right)ds. \tag{26}$$

Then, by substituting (26) into (21), we have

$$p_\tau(t) = \int_t^\tau \frac{\partial F(s)}{\partial \eta}p_s(t)ds + \frac{\partial F(t)}{\partial v}. \tag{27}$$

To make the computation easier to handle, we specify the input signal $v(\tau)$ to be a piecewise constant function of time, i.e., $v(\tau) = v[k]$ for $kT_{\text{s}} \le \tau < (k+1)T_{\text{s}}$ where T_{s} is a sampling period. Then, it can be seen from (27) that $p_\tau(t)$ can be computed as solutions of the following Linear Time Invariant (LTI) system:

$$\frac{dp_\tau(t)}{d\tau} = \frac{\partial F(\tau)}{\partial \eta}p_\tau(t) = (A + BK)p_\tau(t) \tag{28}$$

with the initial condition $p_t(t) = \frac{\partial F(t)}{\partial v} = B$ at $t = kT_{\text{s}} (k = 0, 1, \dots)$. Then, $p_{\tau_{\text{r}}}(t)$ can be calculated by taking the value of $p_\tau(t)$ when $\tau = \tau_{\text{r}}$. Thus, $q(t)$ and $q_{\text{con}}(t)$ can be calculated using (22) and (23) at $t = kT_{\text{s}}$ $(k = 0, 1, \dots)$. Thus, we have computed $q(kT_{\text{s}})$ and $q_{\text{con}}(kT_{\text{s}})$, we specify $q(\tau) = q(kT_{\text{s}})$ and $q_{\text{con}}(\tau) = q_{\text{con}}(kT_{\text{s}})$ for $kT_{\text{s}} \le \tau < (k+1)T_{\text{s}}$.

The functional gradient descent algorithm for the feedforward controller synthesis is shown in Algorithm 1. We denote v^i as the input signals in the ith iteration (similarly, τ_{r}^i and π_{r}^i indicate the critical time and critical proposition in the ith iteration). When the state is in the singular manifold Υ, i.e., $\frac{\partial\sigma(x,z)}{\partial z}$ is not invertible, we perform an SVD decomposition of the matrix $\frac{\partial\sigma(x,z)}{\partial z} = U\Sigma V^*$ and perturb the rank-deficient matrix Σ to be a full-rank matrix $\tilde{\Sigma}$ (line 9). We use the multistart method to avoid the situation when the solution is stuck at one piece of

Algorithm 1: Functional gradient descent algorithm.

1: Simulate the initial trajectory $\xi(\cdot;\eta_0,v^1)$
2: Run `S-TaLiRo` to calculate critical time τ_r^1 and critical proposition π_r^1
3: Calculate $J_{\text{con}}(v^1)$, $i \leftarrow 1$
4: **while** $\big((J_{\text{con}}(v^i) > 0) \vee (\lambda_1 > \epsilon)\big) \wedge (i \leq N_{\max})$ **do**
5: Calculate $p_\tau(t)$ as solution of (28)
6: **if** $\frac{\partial\sigma(x,z)}{\partial z}$ is invertible **then**
7: $\frac{dz}{d\eta} \leftarrow -\big(\frac{\partial\sigma(x,z)}{\partial z}\big)^{-1}\frac{\partial\sigma(x,z)}{\partial x}\frac{dx}{d\eta}$
8: **else**
9: Perform $\frac{\partial\sigma(x,z)}{\partial z} = U\Sigma V^*$ and perturb Σ to be a full-rank matrix $\tilde{\Sigma}$
10: $\frac{dz}{d\eta} \leftarrow -(U\tilde{\Sigma}V^*)^{-1}\frac{\partial\sigma(x,z)}{\partial x}\frac{dx}{d\eta}$
11: **end if**
12: Calculate $q(t)$ and $q_{\text{con}}(t)$ using (22) and (23)
13: **if** $J_{\text{con}}(v^i) \leq 0$ **then**
14: Calculate the input signal of the next iteration $v^{i+1}(\tau) \leftarrow v^i(\tau) - \lambda_1 q(\tau)$
15: Simulate the trajectory of the next iteration $\xi(\cdot;\eta_0,v^{i+1})$
16: Run `S-TaLiRo` to calculate critical time τ_{r}^{i+1}, critical proposition π_{r}^{i+1} and then calculate $J_{\text{con}}(v^{i+1})$
17: Calculate $\hat{J}(v^{i+1}) \leftarrow \sum_{k=0}^{N_T} g(\xi(\tau[k];\eta_0,v^{i+1}), v^{i+1}[k])$
18: **if** $\hat{J}(v^{i+1}) < \hat{J}(v^i)$ **then**
19: $\lambda_1 \leftarrow \alpha\lambda_1, \alpha > 1$
20: **else**
21: $\lambda_1 \leftarrow \beta\lambda_1, 0 < \beta < 1$
22: **end if**
23: **else**
24: Calculate the input signal of the next iteration $v^{i+1}(\tau) \leftarrow v^i(\tau) - \lambda_2 q_{\text{con}}(\tau)$
25: Simulate the trajectory of the next iteration $\xi(\cdot;\eta_0,v^{i+1})$
26: Run `S-TaLiRo` to calculate critical time τ_{r}^{i+1}, critical proposition π_{r}^{i+1} and then calculate $J_{\text{con}}(v^{i+1})$
27: **if** $J_{\text{con}}(v^{i+1}) < J_{\text{con}}(v^i)$ **then**
28: $\lambda_2 \leftarrow \alpha\lambda_2, \alpha > 1$
29: **else**
30: $\lambda_2 \leftarrow \beta\lambda_2, 0 < \beta < 1$
31: **end if**
32: **end if**
33: $i \leftarrow i + 1$
34: **end while**

the constraint manifold when other pieces exist. If the current solution satisfies the constraint, then the next solution will be optimized along the opposite direction of the gradient of the objective function (lines 14–22); otherwise, the next solution will be optimized along the opposite direction of the gradient of the constraint function as the constraint has to be met before the objective function is further minimized (lines 24–31). λ_1 and λ_2 are adjustable stepsizes. For each optimization, the algorithm terminates when the constraint is satisfied ($J_{\text{con}}(v^i) \leq 0$) and the objective function reaches a local minimum ($\lambda_1 \leq \epsilon$), or a maximal number of iterations is exceeded ($i > N_{\max}$).

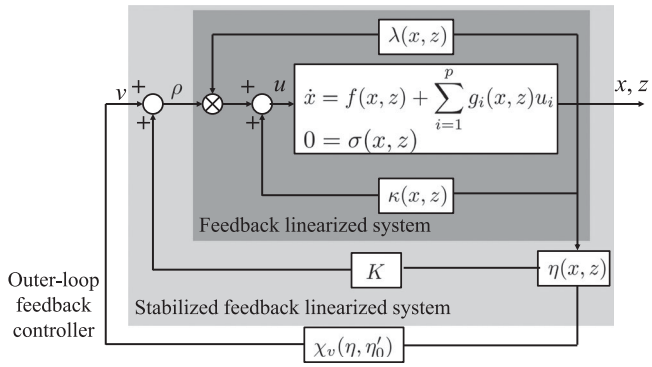

Fig. 3. Diagram of the feedback controller with the stabilized feedback linearized system.

B. Feedback Controller Synthesis

In this section, we design a feedback control law using system identification techniques to replace the optimal input signals of the feedforward controller. When the states and inputs of the trajectories are calculated using numeric simulators such as ODE or CVODE, the data are discrete and therefore in the following we use $\xi_\ell[k] \triangleq \xi_\ell(k;\eta_{0,\ell},v_\ell)$ and $v_\ell[k]$ to denote the flow solution and the input of the ℓth nominal (simulated) trajectory at the kth time instant, respectively. We denote $\mathcal{F} \triangleq \bigcup_{\ell=1}^{N_\ell}\bigcup_{k=0}^{N_{T,\ell}} B_\psi(\xi_\ell[k],\gamma_\ell)$ as the robust neighborhoods around the N_ℓ nominal trajectories ($N_{T,\ell}$ is the number of time points in the ℓth nominal trajectory).

Different from [23], we apply the following piecewise linear feedback law $\chi_v(\eta,\eta_0')$ (as shown in Fig. 3) which depends both on the current state η and the initial state η_0':

$$\chi_v(\eta,\eta_0') \triangleq \begin{cases} \theta_1\eta + \theta_{0,1}, & \text{when } \eta \in \mathcal{X}_1(\eta_0') \\ \theta_2\eta + \theta_{0,2}, & \text{when } \eta \in \mathcal{X}_2(\eta_0') \\ \vdots & \vdots \\ \theta_{n_{\text{c}}}\eta + \theta_{0,n_{\text{c}}}, & \text{when } \eta \in \mathcal{X}_{n_{\text{c}}}(\eta_0') \end{cases} \tag{29}$$

where $\{\mathcal{X}_i(\eta_0')\}_{i=1}^{n_{\text{c}}}$ form a partition of the state space and the partition depends on the initial state η_0'. We use $\xi(k;\eta_0',\chi_v)$ to denote the flow solution of the trajectory starting from η_0' at the kth time instant when the feedback control law $\chi_v(\eta,\eta_0')$ is applied. The feedback control law $\chi_v(\eta,\eta_0')$ and the partition $\{\mathcal{X}_i(\eta_0')\}_{i=1}^{n_{\text{c}}}$ have the following properties (which can be guaranteed using our design approach explained later).

Property 1: For all $k > 0, \ell > 0$, and v_ℓ that satisfies the constraint of (10), if $\xi_\ell[k] \in \mathcal{X}_j(\eta_0')$, then $v_\ell[k] = \theta_j\xi_\ell[k] + \theta_{0,j} - \varepsilon_\ell[k]$, where $\|\varepsilon_\ell[k]\|_\infty \leq \delta$, and

$$\begin{bmatrix} P & (A+BK+B\theta_j)P \\ P^T(A+BK+B\theta_j)^T & P \end{bmatrix} \succeq 0. \tag{30}$$

Property 2: If $\eta \in \mathcal{F} \cap \mathcal{X}_j(\eta_0')$, then there exists a $\xi_\ell[k] \in \mathcal{X}_j(\eta_0')$ such that $\eta \in B_\psi(\xi_\ell[k],\gamma_\ell)$.

Property 3: For any $\eta_0' \in \bigcup_{\ell=1}^{N_\ell} B_\psi(\eta_{0,\ell}, \gamma_\ell)$, if $\ell' = \min\{\ell | \eta_0' \in B_\psi(\eta_{0,\ell}, \gamma_\ell)\}$, then for all $k > 0$, if $\xi_{\ell'}[k] \in \mathcal{X}_j(\eta_0')$, then $\xi(k; \eta_0', \chi_v) \in \mathcal{X}_j(\eta_0')$.

Remark 1: Properties 1, 2 are modified from [23] while Property 3 is added in this paper as MTL specifications requires more stringent conditions than safety specifications in [23].

Theorem 1: If the feedback control law $\chi_v(\eta, \eta_0')$ and the partition $\{\mathcal{X}_i(\eta_0')\}_{i=1}^{n_c}$ have Properties 1, 2, and 3, then there exists a critical radius $\gamma_{\text{crit}} > 0$ such that if $\min_{1\le\ell\le N_\ell} \gamma_\ell > \gamma_{\text{crit}}$, the following is true for all $\eta_0' \in \bigcup_{\ell=1}^{N_\ell} B_\psi(\eta_{0,\ell}, \gamma_\ell)$ and $k > 0$: $\ell' = \min\{\ell | \eta_0' \in B_\psi(\eta_{0,\ell}, \gamma_\ell)\} \Rightarrow \psi(\xi_{\ell'}[k], \xi(k; \eta_0', \chi_v)) \le \gamma_{\ell'}$.

Proof: Straightforward from Theorem 1, Theorem 4, and the analysis part in the right column of [23, p. 4] while applying Properties 1–3. ■

It can be seen from Theorem 1 that if $\chi_v(\eta, \eta_0')$ and $\{\mathcal{X}_i(\eta_0')\}_{i=1}^{n_c}$ have Properties 1–3 and $\min_{1\le\ell\le N_\ell} \gamma_\ell > \gamma_{\text{crit}}$, then any trajectory that starts from the initial set $B_\psi(\eta_{0,\ell'}, \gamma_{\ell'}) \setminus \bigcup_{\ell<\ell'} B_\psi(\eta_{0,\ell}, \gamma_\ell)$ when $\chi_v(\eta, \eta_0')$ is applied will remain in the robustness ellipsoids $B_\psi(\xi_{\ell'}[k], \gamma_{\ell'})$.

Theorem 2: Assume that $x(\eta)$ is Lipschitz continuous for $\eta \in \mathcal{F}$, i.e., $\|x(\eta_1) - x(\eta_2)\| \le K_x \|\eta_1 - \eta_2\|$ for any η_1, $\eta_2 \in \mathcal{F}$, and some constant $K_x > 0$. If the feedback control law $\chi_v(\eta, \eta_0')$ and the partition $\{\mathcal{X}_i(\eta_0')\}_{i=1}^{n_c}$ have Properties 1–3, then there exists a critical radius $\gamma_{\text{crit}} > 0$ such that if $\min_{1\le\ell\le N_\ell} \gamma_\ell > \gamma_{\text{crit}}$ and $\max_{1\le\ell\le N_\ell} \gamma_\ell \|P^{-\frac{1}{2}}\| K_x \le \zeta$ ($\|P^{-\frac{1}{2}}\|$ is the largest singular value of $P^{-\frac{1}{2}}$), then the trajectory $x(\xi(\cdot; \eta_0', \chi_v))$ satisfies the MTL specification ϕ for any $\eta_0' \in \bigcup_{\ell=1}^{N_\ell} B_\psi(\eta_{0,\ell}, \gamma_\ell)$.

Proof: As $\eta_0' \in \bigcup_{\ell=1}^{N_\ell} B_\psi(\eta_{0,\ell}, \gamma_\ell)$, if $\ell' = \min\{\ell | \eta_0' \in B_\psi(\eta_{0,\ell}, \gamma_\ell)\}$, according to Theorem 1, for all $k > 0$, $\psi(\xi_{\ell'}[k], \xi(k; \eta_0', \chi_v)) = [(\xi_{\ell'}[k] - \xi(k; \eta_0', \chi_v))^T P (\xi_{\ell'}[k] - \xi(k; \eta_0', \chi_v))]^{\frac{1}{2}} \le \gamma_{\ell'}$, thus $\|\xi_{\ell'}[k] - \xi(k; \eta_0', \chi_v)\| \le \gamma_{\ell'} \|P^{-\frac{1}{2}}\|$. As for all $k > 0$, $\xi_{\ell'}[k] \in \mathcal{F}$, $\xi(k; \eta_0', \chi_v) \in \mathcal{F}$, so $\|x(\xi_{\ell'}[k]) - x(\xi(k; \eta_0', \chi_v))\| \le K_x \|\xi_{\ell'}[k] - \xi(k; \eta_0', \chi_v)\| \le K_x \gamma_{\ell'} \|P^{-\frac{1}{2}}\|$. Therefore, if $[[\phi]](x(\xi_{\ell'}[\cdot]), 0) \ge \zeta$ (from (10), here $x(\xi_{\ell'}[\cdot])$ denotes a discrete-time trajectory) and $K_x \gamma_{\ell'} \|P^{-\frac{1}{2}}\| \le \max_{1\le\ell\le N_\ell} \gamma_\ell \|P^{-\frac{1}{2}}\| K_x \le \zeta$, then $[[\phi]](x(\xi_{\ell'}[\cdot]), 0) \ge \max_{k>0} \|x(\xi_{\ell'}[k]) - x(\xi(k; \eta_0', \chi_v))\|$, thus using the triangle inequality it can be proven that $[[\phi]](x(\xi(\cdot; \eta_0', \chi_v)), 0) \ge 0$. ■

In order to satisfy Properties 1–3, in the following we describe the clustering, partitioning, and boundary modification process to determine $\{\mathcal{X}_i(\eta_0')\}_{i=1}^{n_c}$ and $\chi_v(\eta, \eta_0')$.

1) Clustering: The basic idea of the clustering algorithm is to find θ_i and $\theta_{0,i}$ that make the inequalities $|\theta_i \xi_\ell[k] + \theta_{0,i} - v_\ell[k]| \le \delta$ true for as many k and ℓ as possible (maximum feasible subsystem problem), then remove those points and repeat the same process over the remaining ones until all points have been covered (for details, see [24]). For $i \ge 2$, θ_i and $\theta_{0,i}$ are also tested in the place of θ_j and $\theta_{0,j}$ ($j < i$) in the previous coverings. If θ_i and $\theta_{0,i}$ can cover more points than θ_j and $\theta_{0,j}$, then θ_j and $\theta_{0,j}$ will be replaced by θ_i and $\theta_{0,i}$ to prevent the suboptimality of the greedy algorithm. For each candidate θ_i and $\theta_{0,i}$, we also check if (30) is satisfied to make sure that Property 1 is satisfied. The clusters are further split into subclusters (by *k*-means or other clustering methods) until the convex hull of each subcluster is disjoint with the convex hull of any other subcluster.

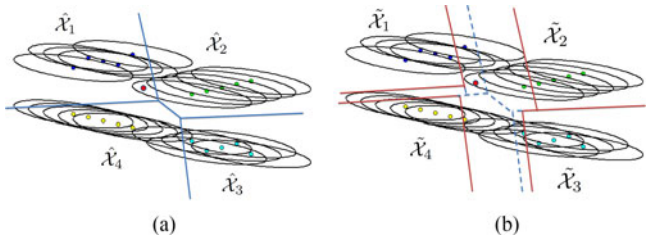

Fig. 4. Piecewise linear classifiers of four sets of points with robustness ellipsoids around them (left) and the reduced partitions with modified boundaries (right).

2) Partitioning: After all the disjoint subclusters are obtained, we classify all the subclusters using multiclass linear classification. There are two major approaches of multiclass linear classification: pairwise linear classifiers and piecewise linear classifiers. The pairwise linear classifiers classify each class with every other class and then use the intersection of all the half spaces determined by the pairwise decision boundaries as the partition for the class. It is easy to implement, but it is not guaranteed to form a complete partition of the whole state space as there may be "holes" that do not belong to any partition [24]. The piecewise linear classifier can form a complete partition of the whole state space and therefore is a better fit for our approach. There are several different methods of constructing piecewise linear classifiers. One way is to construct n_c classification functions for the n_c subclasses such that at each data point the corresponding class function is maximal. We use robust LP to find the n_c classification functions for the n_c subclasses.

Definition 3 ([32]): The n_c sets $\mathcal{A}^i (i = 1, 2, \ldots, n_c)$, each consisting of m_c^i points in $\mathbb{R}^n$ and represented by the $n \times m_c^i$ matrices A^i, are piecewise linear separable if there exists $\vartheta^i, \vartheta^j \in \mathbb{R}^n, b^i, b^j \in \mathbb{R}$ such that

$$\vartheta^i A^i - e b^i > \vartheta^j A^i - e b^j, \quad i, j = 1, 2, \ldots, n_c, i \ne j \tag{31}$$

where e is a vector of ones.

The classification problem becomes the following LP problem:

$$\begin{aligned} \min_{\vartheta^i, b^i, y^{ij}} & \sum_{i=1}^{n_c} \sum_{j=1, j\ne i}^{n_c} \frac{e y^{ij}}{m_c^i} \\ \text{s.t. } & y^{ij} \ge -(\vartheta^i - \vartheta^j) A^i + e(b^i - b^j) + e \\ & y^{ij} \ge 0, i, j = 1, 2, \ldots, n_c, i \ne j. \end{aligned} \tag{32}$$

3) Boundary modification: We denote the resulting partition of the above LP optimization as $\{\hat{\mathcal{X}}_i\}_1^{n_c}$. As shown in Fig. 4(a), the red point does not belong to any robustness ellipsoid within the partition $\hat{\mathcal{X}}_1$, but belongs to a robustness ellipsoid in another partition $\hat{\mathcal{X}}_2$ (Property 2 is violated). To avoid this, each partition is shrunk so that it does not intersect any robustness ellipsoid outside the partition, as shown in the shrunken partitions enclosed by the brown lines in Fig. 4(b). In the meantime, for each partition face, we make note of the robustness ellipsoids centered outside the partition and intersect the partition face. Let $S_{ij} \triangleq \{(\ell, k) | - \|(\vartheta^i - \vartheta^j) P^{-\frac{1}{2}}\| \gamma_\ell <$

$(\vartheta^i - \vartheta^j)\xi_\ell[k] + b^i - b^j < 0\}$ be the set of pairs (ℓ, k) where the robustness ellipsoid of the ℓth simulated trajectory at the kth time instant (outside of $\hat{\mathcal{X}}_i$) intersects the decision boundary between the ith and jth subcluster of data. We calculate $b_{ij}^- \triangleq \min_{(\ell,k)\in S_{ij}}(-\|(\vartheta^i - \vartheta^j)P^{-\frac{1}{2}}\|\gamma_\ell - (\vartheta^i - \vartheta^j)\xi_\ell[k])$, and thus, obtain the new decision boundary $(\vartheta^i - \vartheta^j)x + b_{ij}^- = 0$. Thus, we obtain a reduced partition $\tilde{\mathcal{X}}_i$ for each original partition $\hat{\mathcal{X}}_i$ such that a system state within $\tilde{\mathcal{X}}_i$ is guaranteed not to belong to a robustness ellipsoid in any other partitions.

When implemented online, given the initial state η_0', we first calculate $\ell' = \min\{\ell | \eta_0' \in B_\psi(\eta_{0,\ell}, \gamma_\ell)\}$, then we use the following algorithm to determine the final partition $\{\mathcal{X}_i(\eta_0')\}_{i=1}^{n_c}$ and the feedback control law $\chi_v(\eta, \eta_0')$.

1) If the current state η lies within the reduced partition $\tilde{\mathcal{X}}_i$, then $\eta \in \mathcal{X}_i(\eta_0')$, the feedback control law $\chi_v(\eta, \eta_0') = \theta_i\eta + \theta_{0,i}$ is applied.
2) If the current state lies within the original partition $\hat{\mathcal{X}}_i$, but not the reduced partition $\tilde{\mathcal{X}}_i$, check to see if it lies within any of the robustness ellipsoids marked in $S_{ij}(j \neq i)$, then:
   a) if it does not lie within any robustness ellipsoid centered outside of $\hat{\mathcal{X}}_i$, then $\eta \in \mathcal{X}_i(\eta_0')$, the feedback control law $\chi_v(\eta, \eta_0') = \theta_i\eta + \theta_{0,i}$ is applied;
   b) if it lies within a unique robustness ellipsoid centered at $\xi_\ell[k]$ and $\xi_\ell[k]$ lies within the jth partition $(j \neq i)$, then $\eta \in \mathcal{X}_j(\eta_0')$, the feedback control law $\chi_v(\eta, \eta_0') = \theta_j\eta + \theta_{0,j}$ is applied;
   c) if it lies within more than one robustness ellipsoids, find the partition $\hat{\mathcal{X}}_w$ where the state $\xi_{\ell'}[k]$ lies (k is the current time instant), then $\eta \in \mathcal{X}_w(\eta_0')$, the feedback control law $\chi_v(\eta, \eta_0') = \theta_w\eta + \theta_{0,w}$ is applied (in this way, Property 3 is always satisfied).

IV. Energy Storage Controller Synthesis

In this section, we apply the controller synthesis method in designing an energy storage controller for regulating the grid frequency of a double-machine infinite-bus system as shown in Fig. 5 [33]. Two synchronous generators are denoted as G_i ($i = 1, 2$), two constant power loads are denoted as L_1 and L_2, and two constant impedance loads are denoted as L_3 and L_4. Two ESSs are placed near G_1 and G_2. The configuration parameters of the power system model and the line data can be seen in Tables I and II. The swing dynamics of machine G_i ($i = 1, 2$) can be described by the following classical model:

$$\begin{cases} \dot{\delta}_i = \omega_i \\ \frac{P_{ri}}{P_b}\frac{H_i}{\pi f_s}\dot{\omega}_i = P_{mi} - P_{ESSi} - D_i\omega_i - p_{ei} \end{cases} \tag{33}$$

where δ_i is the rotor angle position of G_i with respect to the infinite bus at G_3, ω_i is the rotor speed deviation of G_i relative to system angular frequency $2\pi f_s$, P_b is the base power in the per unit system, P_{ri} is the rated power of G_i, H_i is the per-unit inertia constant, P_{mi} is the mechanical input power to G_i, D_i is the damping coefficient, P_{ESSi} is the power that flows from the grid to the ESS near G_i, the electrical output power P_{ei} is described by the following function of δ_1, δ_2 ($\delta_3 = 0$ in the following equation):

$$P_{ei} \triangleq \sum_{j=1}^{3} E_iE_j\{G_{ij}\cos(\delta_i - \delta_j) + B_{ij}\sin(\delta_i - \delta_j)\} + \sum_{j=1}^{2} E_iV_j\{\hat{G}_{ij}\cos(\delta_i - \theta_j) + \hat{B}_{ij}\sin(\delta_i - \theta_j)\} \tag{34}$$

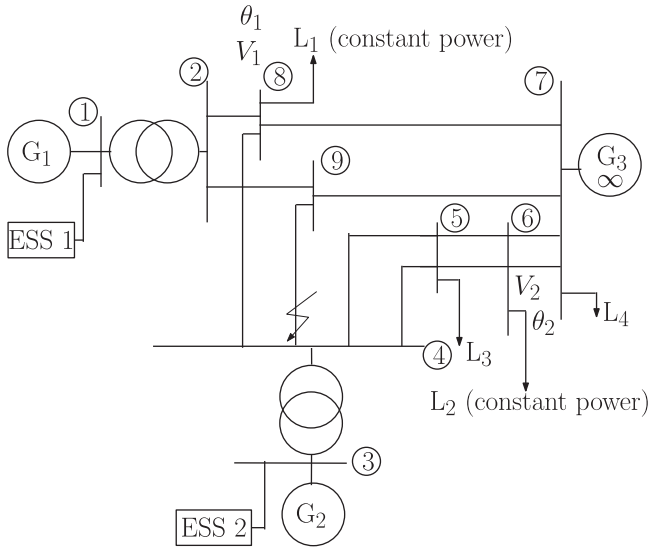

Fig. 5. Double-machine infinite-bus system.

TABLE I
System Parameters

VA base P_b		160 MVA
System frequency f_s		60 Hz
Machine rating P_{ri} of G_i	$i = 1$	82 MVA
	$i = 2$	160 MVA
Mechanical input power P_{mi}	$i = 1$	0.28 (p.u.)
	$i = 2$	0.75 (p.u.)
Active power flow to load L_i	$i = 1$	0.25 (p.u.)
	$i = 2$	0.4375 (p.u.)
	$i = 3$	0.1875 (p.u.)
	$i = 4$	0.75 (p.u.)
Transient reactance of G_i	$i = 1$	0.261 (p.u.)
	$i = 2$	0.284 (p.u.)
Per-unit inertia constant H_i	$i = 1$	5 s
	$i = 2$	3.5 s
Damping coefficient D_i of G_i	$i = 1, 2$	0.01 s
Voltage E_i of G_i	$i = 1, 2$	1.05 (p.u.)
Transformer impedance	G_1	1.8868 (p.u.)
	G_2	0.618 (p.u.)

TABLE II
Line Data (160 MVA Base)

Line number	Line impedance (p.u.)	Line charging (p.u.)
2–8(2–9)	0.0224 + j0.1051	0.0006625
7–8(7–9)	0.0880 + j0.4080	0.0023
4–8(4–9)	0.1168 + j0.5440	0.0031
4–5	0.0015 + j0.0029	0.0034
5–6	0.0023 + j0.0032	0.0094
6–7	0.0053 + j0.0201	0.0258

where E_i is the voltage behind the transient reactance of G_i, G_{ii} is its internal conductance, $G_{ij}+jB_{ij}$ is the transfer admittance between G_i and G_j, $\hat{G}_{ij}+j\hat{B}_{ij}$ is the transfer admittance between G_i and L_j, V_j and θ_j are the bus voltage and bus phase angle of $\mathrm{L}_j\,(j=1,2)$, respectively.

The power balance equations for the constant power loads are as follows ($\delta_3=0$ in the following equations):

$$\begin{aligned}0 &= P_{\mathrm{d}i}+\sum_{j=1}^{3}V_iE_j\{\hat{G}_{ji}\cos(\theta_i-\delta_j)+\hat{B}_{ji}\sin(\theta_i-\delta_j)\}\\ &\quad+\sum_{j=1}^{2}V_iV_j\{\tilde{G}_{ij}\cos(\theta_i-\theta_j)+\tilde{B}_{ij}\sin(\theta_i-\theta_j)\}\\ 0 &= Q_{\mathrm{d}i}+\sum_{j=1}^{3}V_iE_j\{\hat{G}_{ji}\sin(\theta_i-\delta_j)-\hat{B}_{ji}\cos(\theta_i-\delta_j)\}\\ &\quad+\sum_{j=1}^{2}V_iV_j\{\tilde{G}_{ij}\sin(\theta_i-\theta_j)-\tilde{B}_{ij}\cos(\theta_i-\theta_j)\}\end{aligned}\tag{35}$$

where $P_{\mathrm{d}i}$ and $Q_{\mathrm{d}i}$ are the real power and reactive power of constant power load L_i $(i=1,\,2)$, $\hat{G}_{ji}+j\hat{B}_{ji}$ is the transfer admittance between G_j and L_i, $\tilde{G}_{ij}+j\tilde{B}_{ij}$ is the transfer admittance between L_i and L_j $(i,j=1,2)$.

We use the following MTL specification for frequency regulation (here time zero represents the fault clearing time):

$$\begin{aligned}\phi &= \Box\neg\phi_1\wedge\Box\neg\phi_2\wedge\Box_{[2,T]}\phi_3\wedge\Box_{[2,T]}\phi_4\\ \phi_1 &= (\omega_1>10),\phi_2=(\omega_2>10)\\ \phi_3 &= (-2\le\omega_1\le 2)\wedge(-2\le\omega_2\le 2)\wedge(-\pi/2\le\delta_1\le\pi/2)\\ &\quad\wedge(-\pi/2\le\delta_2\le\pi/2)\end{aligned}$$

which reads "The frequency deviations should never exceed 10 rad/s, after 2 s the frequency deviations should always be within ±2 rad/s and machine angles should always be within $\pm\pi/2$."

Assume that a three-phase lines-to-ground fault occurs near bus 4 on lines 4–9 and the resulting fault-on system dynamics is as follows:

$$\begin{cases}\dot{x}_1 = x_3\\ \dot{x}_2 = x_4\\ \dot{x}_3 = 74.3059\big(0.28-0.01x_3-(0.0027808-0.00045389\\ \quad\cdot\cos(x_1)+0.054597\sin(x_1)-0.0020063z_3\\ \quad\cdot\cos(x_1-z_1)+0.30751z_3\sin(x_1-z_1))\big)\\ \dot{x}_4 = 53.8559\big(0.75-0.01x_4\big)\end{cases}$$

$$\begin{cases}0 = -0.25-(0.0020063z_3\cos(z_1-x_1)+0.30751z_3\\ \quad\cdot\sin(z_1-x_1)-0.76927z_3\cos(z_1)+3.5329z_3\sin(z_1)\\ \quad+1.3459z_3^2)\\ 0 = -0.4375-(-12.1574z_4\cos(z_2)+46.4191z_4\sin(z_2)\\ \quad+84.8243z_4^2)\\ 0 = 0.0020063z_3\sin(z_1-x_1)-0.30751z_3\cos(z_1-x_1)\\ \quad-0.76927z_3\sin(z_1)-3.5329z_3\cos(z_1)+6.4861z_3^2\\ 0 = -12.157z_4\sin(z_2)-46.419z_4\cos(z_2)+164.647z_4^2\end{cases}$$

where the state $x=[\delta_1,\delta_2,\omega_1,\omega_2]^T$, $z=[\theta_1,\theta_2,V_1,V_2]^T$.

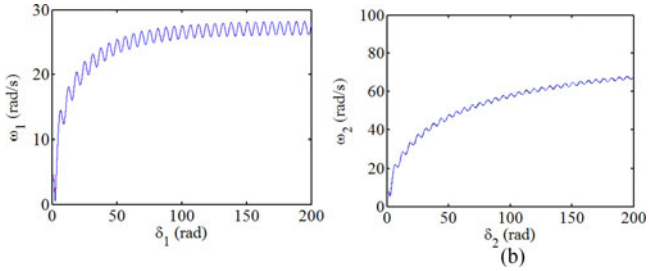

Fig. 6. Simulated postfault trajectories with no storage input with fault clearing time of 0.19 and 0.2 s.

After the fault is cleared, the postfault system with the input $u=[P_{\mathrm{ESS1}},P_{\mathrm{ESS2}}]^T$ is as follows:

$$\begin{cases}\dot{x}_1 = x_3\\ \dot{x}_2 = x_4\\ \dot{x}_3 = 74.3059\big(0.28-u_1-0.01x_3-(0.003-0.00062\\ \quad\cdot\cos(x_1)+0.0683\sin(x_1)-0.00237z_3\cos(x_1-z_1)\\ \quad+0.3336z_3\sin(x_1-z_1))\big)\\ \dot{x}_4 = 53.8559\big(0.75-u_2-0.01x_4-(0.00447+0.00455z_3\\ \quad\cdot\cos(x_2-z_1)+0.0134z_3\sin(x_2-z_1)-0.0083z_4\\ \quad\cdot\cos(x_2-z_2)+1.0875z_4\sin(x_2-z_2))\big)\end{cases}$$

$$\begin{cases}0 = -0.25-(-0.0023695z_3\cos(z_1-x_1)+0.3336z_3\\ \quad\cdot\sin(z_1-x_1)+0.00455z_3\cos(z_1-x_2)+0.013353z_3\\ \quad\cdot\sin(z_1-x_2)-0.84z_3\cos(z_1)+3.83z_3\sin(z_1)+1.47\\ \quad-0.38326z_3z_4\cos(z_1-z_2)+1.7208z_3z_4\sin(z_1-z_2))\\ 0 = -0.4375-(-0.008316z_4\cos(z_2-x_2)+1.0875z_4\\ \quad\cdot\sin(z_2-x_2)-12.1574z_4\cos(z_2)+46.4191z_4\sin(z_2)\\ \quad-0.38326z_3z_4\cos(z_2-z_1)+1.7208z_3z_4\sin(z_2-z_1)\\ \quad+13.1715z_4^2)\\ 0 = -0.0023695z_3\sin(z_1-x_1)-0.3336z_3\cos(z_1-x_1)\\ \quad+0.0045526z_3\sin(z_1-x_2)-0.013353z_3\cos(z_1-x_2)\\ \quad-0.83677z_3\sin(z_1)-3.8322z_3\cos(z_1)+5.8948z_3^2\\ \quad-0.38326z_3z_4\sin(z_1-z_2)-1.7208z_3z_4\cos(z_1-z_2)\\ 0 = -0.008316z_4\sin(z_2-x_2)-1.0875z_4\cos(z_2-x_2)\\ \quad-12.1574z_4\sin(z_2)-46.4191z_4\cos(z_2)-0.3833z_3z_4\\ \quad\cdot\sin(z_2-z_1)-1.7208z_3z_4\cos(z_2-z_1)+49.1724z_4^2.\end{cases}$$

We assume that the fault is cleared between 0.19 and 0.2 s. As shown in Fig. 6, the postfault system with no storage input ($u_1=u_2=0$) is not stable as the two generators lose synchronism soon after the fault is cleared. Therefore, an energy storage controller is necessary not only for the purpose of frequency regulation, but also for maintaining the transient stability of the postfault system.

We first feedback linearize the postfault system using the M derivative. By choosing the output functions as $h_1(x,z)=x_1, h_2(x,z)=x_2$, the postfault feedback linearized system is as follows:

$$\begin{cases}\dot{\eta}_1 = \eta_2\\ \dot{\eta}_2 = \rho_1\\ \dot{\eta}_3 = \eta_4\\ \dot{\eta}_4 = \rho_2\end{cases}$$

where the new state $\eta = [x_1, x_3, x_2, x_4]^T$, $\rho = [\rho_1, \rho_2]^T$ is the input of the feedback linearized system. $\kappa(x, z)$ and $\lambda(x, z)$ in (4) are calculated as follows:

$$\lambda(x,z) = \begin{bmatrix} -\frac{1}{74.3059} & 0 \\ 0 & -\frac{1}{53.8559} \end{bmatrix}$$

$$\kappa(x,z) = \begin{bmatrix} 0.28 - 0.01x_3 - (0.003 - 0.00062\cos(x_1) \\ +0.0683\sin(x_1) - 0.00237z_3\cos(x_1 - z_1) \\ +0.3336z_3\sin(x_1 - z_1)); \\ 0.75 - 0.01x_4 - (0.00447 + 0.00455z_3 \\ \cdot\cos(x_2 - z_1) + 0.0134z_3\sin(x_2 - z_1) - 0.0083 \\ \cdot z_4\cos(x_2 - z_2) + 1.0875z_4\sin(x_2 - z_2)) \end{bmatrix}.$$

We then introduce input v and let $\rho(\eta) = K\eta + v$, where

$$K = \begin{bmatrix} -0.8068 & -0.9894 & 0 & 0 \\ 0 & 0 & -0.8068 & -0.9894 \end{bmatrix}$$

is calculated using (9). The obtained system $\dot{\eta} = F(\eta, v) = (A + BK)\eta + Bv$ is a stabilized linear system with the new input v.

To optimize v for the feedforward controller synthesis, we use Algorithm 1 and set $T = 10$ s, $T_s = 0.1$ s, $\zeta = 0.3$, $N_{\max} = 100$, $\epsilon = 10^{-6}$, $\lambda_1 = \lambda_2 = 1$ (initial values), $\alpha = 1.5$, $\beta = 0.2$ (all the values are per unit values unless otherwise specified). We simulate three trajectories of the postfault feedback linearized system starting from the fault-on trajectories cleared at 0.1912 s, 0.195 s, and 0.1995 s respectively. The optimal input signal v and the corresponding storage input u for the three different fault clearing time are shown in Fig. 7. It can be seen that in all three different scenarios, the power flows from the grid to the ESSs near G_1 and G_2 significantly in the first 1 to 2 s to decrease the grid frequency. After this period, the power flow changes direction as the frequency deviation becomes negative and continues to decrease, so the ESSs have to inject power to the grid to prevent the frequency from dropping beyond the lower threshold. After the first 5 s, the storage control efforts gradually decrease to zero. It can also be seen that with longer fault clearing time, more (storage) control effort is needed to satisfy the MTL specification ϕ.

The initial robustness ellipsoid of the simulated postfault trajectory with fault clearing time of 0.195 s totally covers the simulated fault-on trajectory from 0.19 to 0.2 s (the postfault initial states), as shown in Fig. 8. Thus, all the possible postfault trajectories with the given uncertainties in the fault clearing time (between 0.19 and 0.2 s) are guaranteed to satisfy the MTL specification ϕ (as shown in Fig. 9).

Next, we design a piecewise linear feedback law that is learned from the data of the simulated trajectory and the corresponding optimal inputs. We first cluster the 1001 data points into 94 disjoint subclusters while in each subcluster the input error is within $\delta = 0.0118$ (as γ_{crit} depend on δ [23], δ is designed such that $\min_{1\le\ell\le N_\ell}\gamma_\ell > \gamma_{\text{crit}}$ and $\max_{1\le\ell\le N_\ell}\gamma_\ell\|P^{-\frac{1}{2}}\|K_x \le \zeta$, here $N_\ell = K_x = 1$), as shown in Fig. 10. We generate the piecewise linear classifier to separate the 94 subclusters and modify the partitions using the method described in Section III-B. We generate 20 postfault trajectories with the

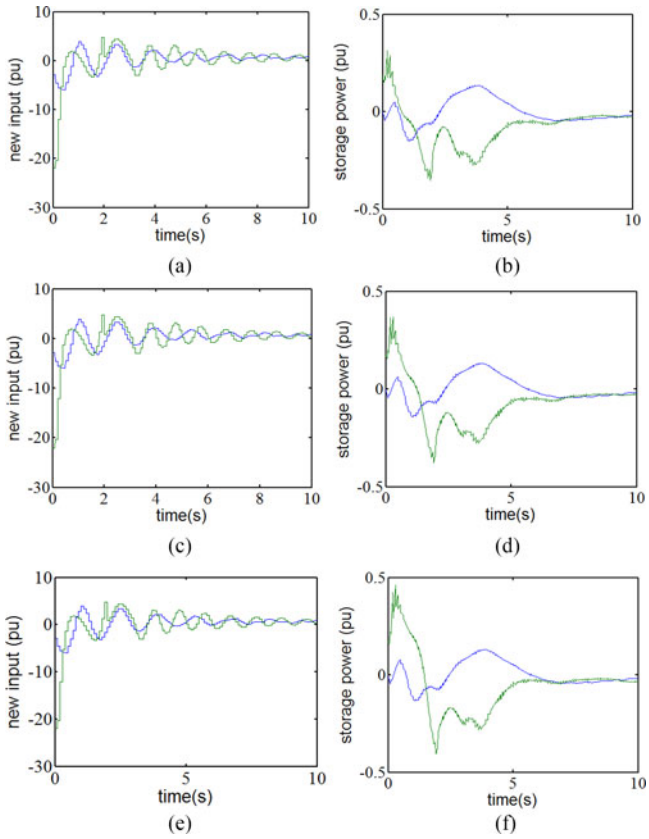

Fig. 7. New input v and storage input u (blue for ESS 1 and green for ESS 2) of the feedforward controller with fault clearing time of: (a), (b) 0.1912 s, (c), (d) 0.195 s, (e), (f) 0.1995 s.

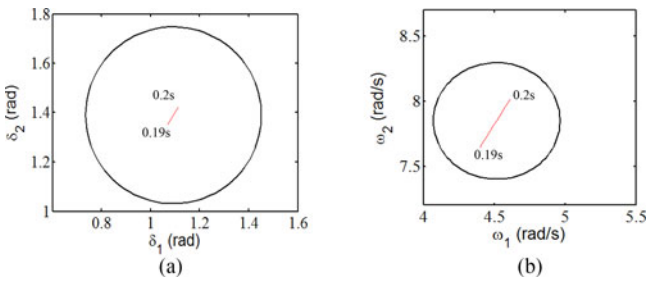

Fig. 8. Coverage of the simulated fault-on trajectory from 0.19 to 0.2 s (red) with the initial robustness ellipsoid (black) of the simulated postfault trajectory with fault clearing time of 0.195 s.

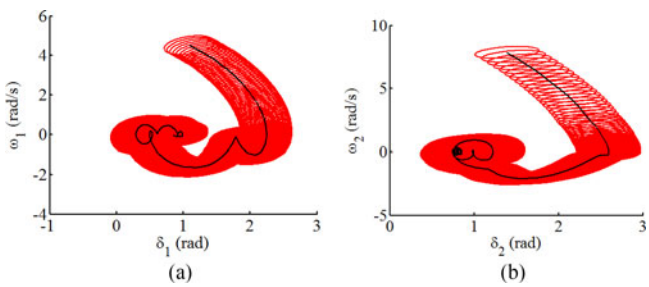

Fig. 9. Robust neighborhoods (red) of the nominal (simulated) postfault trajectory (black) with fault clearing time of 0.195 s.

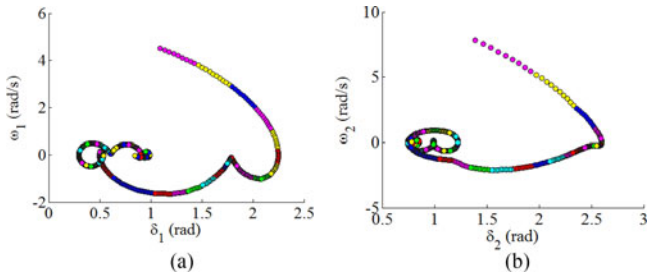

Fig. 10. Subclusters obtained from the bounded-error clustering approach (different colors represent different subclusters).

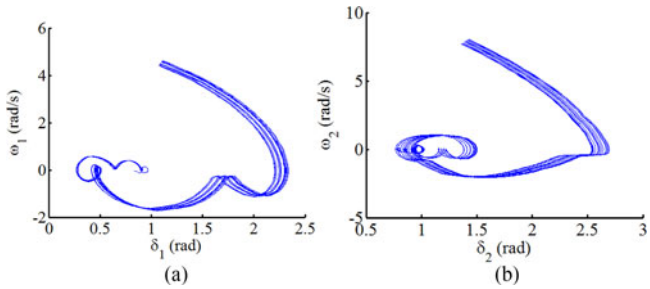

Fig. 11. Twenty postfault trajectories generated with the feedback controller over a sampling of initial conditions (fault clearing time between 0.19 and 0.2 s).

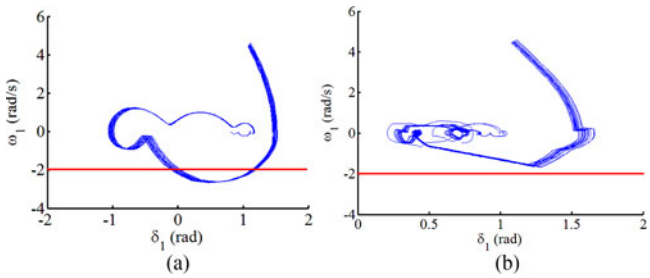

Fig. 12. Twenty postfault trajectories generated with the feedforward controller (a) and the feedback controller, (b) over a sampling of initial conditions (fault clearing time between 0.19 and 0.2 s) with the disturbance of value -20 in the first dimension of the input v during the first 0.2 s.

feedback controller over a sampling of initial conditions and the trajectories all satisfy the MTL specification ϕ (as shown in Fig. 11).

To make a comparison between the feedback controller and the feedforward controller, we add a disturbance of value -20 to the first dimension of the input v during the first 0.2 s while generating the 20 postfault trajectories with both the feedforward and the feedback controllers over a sampling of initial conditions (fault clearing time between 0.19 and 0.2 s). As shown in Fig. 12(a), with the feedforward controller, although the rotor speed deviation ω_1 still gradually approaches zero, ω_1 crosses -2 rad/s in the process as the inputs are precomputed and thus unresponsive to the unexpected disturbance. In comparison, as shown in Fig. 12(b), with the feedback controller, the rotor speed deviation ω_1 is always greater than -2 rad/s as the feedback controller adjusts the inputs according to the feedback law, thus the states remain in the robust neighborhoods $\mathcal{F}$ despite the unexpected disturbances.

V. Conclusion

We presented a controller synthesis framework to control the ESSs with MTL specifications. We model the power system as a nonlinear DAE system and both the feedforward and the feedback controller synthesis for such DAE systems are presented. The controller synthesis approach can be used in other related areas in power systems such as transient stability enhancement, voltage regulation, etc. Similar approaches can be also applied to other nonlinear DAE systems such as robotic systems, biological systems, etc.

Acknowledgment

The authors would like to thank Dr. A. K. Winn for helpful discussions.

References

[1] F. Delfino, F. Pampararo, R. Procopio, and M. Rossi, "A feedback linearization control scheme for the integration of wind energy conversion systems into distribution grids," *IEEE Syst. J.*, vol. 6, no. 1, pp. 85–93, Mar. 2012.

[2] Z. Xu, A. A. Julius, and J. H. Chow, "Robust testing of cascading failure mitigations based on power dispatch and quick-start storage," *IEEE Syst. J.*, to be published.

[3] A. D. Papalexopoulos and P. E. Andrianesis, "Performance-based pricing of frequency regulation in electricity markets," *IEEE Trans. Power Syst.*, vol. 29, no. 1, pp. 441–449, Jan. 2014.

[4] A. Mondal, S. Misra, and M. S. Obaidat, "Distributed home energy management system with storage in smart grid using game theory," *IEEE Syst. J.*, vol. 11, no. 3, pp. 1857–1866, Sep. 2017.

[5] S. W. Mohod and M. V. Aware, "Micro wind power generator with battery energy storage for critical load," *IEEE Syst. J.*, vol. 6, no. 1, pp. 118–125, Mar. 2012.

[6] A. K. Srivastava, A. A. Kumar, and N. N. Schulz, "Impact of distributed generations with energy storage devices on the electric grid," *IEEE Syst. J.*, vol. 6, no. 1, pp. 110–117, Mar. 2012.

[7] Z. Xu, C. Belta, and A. A. Julius, "Temporal logic inference with prior information: An application to robot arm movements," *IFAC-PapersOnLine*, vol. 48, no. 27, pp. 141–146, 2015.

[8] Z. Xu, M. Birtwistle, C. Belta, and A. Julius, "A temporal logic inference approach for model discrimination," *IEEE Life Sci. Lett.*, vol. 2, no. 3, pp. 19–22, Sep. 2016.

[9] P. Tabuada, *Verification and Control of Hybrid Systems: A Symbolic Approach*. New York, NY, USA: Springer, 2009. [Online]. Available: https://books.google.com/books?id=1ExhrqtzIYwC

[10] E. M. Wolff, U. Topcu, and R. M. Murray, "Automaton-guided controller synthesis for nonlinear systems with temporal logic," in *Proc. IEEE/RSJ Int. Conf. Intell. Robots Syst.*, Nov. 2013, pp. 4332–4339.

[11] S. Coogan, E. A. Gol, M. Arcak, and C. Belta, "Traffic network control from temporal logic specifications," *IEEE Trans. Control Netw. Syst.*, vol. 3, no. 2, pp. 162–172, Jun. 2016.

[12] A. Donzé and V. Raman, "Blustl: Controller synthesis from signal temporal logic specifications," in ARCH@CPSWeek, 2015.

[13] S. Saha and A. A. Julius, "An MILP approach for real-time optimal controller synthesis with metric temporal logic specifications," in *Proc. IEEE Amer. Control Conf.*, Jul. 2016, pp. 1105–1110.

[14] A. K. Winn and A. A. Julius, "Optimization of human generated trajectories for safety controller synthesis," in *Proc. IEEE Amer. Control Conf.*, Jun. 2013, pp. 4374–4379.

[15] H. Abbas, A. Winn, G. Fainekos, and A. A. Julius, "Functional gradient descent method for metric temporal logic specifications," in *Proc. IEEE Amer. Control Conf.*, Jun. 2014, pp. 2312–2317.

[16] S. Sastry and C. Desoer, "Jump behavior of circuits and systems," *IEEE Trans. Circuits Syst.*, vol. 28, no. 12, pp. 1109–1124, Dec. 1981.

[17] D. Karimipour and F. R. Salmasi, "Stability analysis of ac microgrids with constant power loads based on popov's absolute stability criterion," *IEEE Trans. Circuits Syst. II, Express Briefs*, vol. 62, no. 7, pp. 696–700, Jul. 2015.

[18] X. Lu, K. Sun, J. M. Guerrero, J. C. Vasquez, L. Huang, and J. Wang, "Stability enhancement based on virtual impedance for dc microgrids with constant power loads," *IEEE Trans. Smart Grid*, vol. 6, no. 6, pp. 2770–2783, Nov. 2015.
[19] Y. Li and J. Liu, "Switching control of differential-algebraic equations with temporal logic specifications," in *Proc. IEEE Amer. Control Conf.*, Jul. 2015, pp. 1941–1946.
[20] M. Althoff and B. H. Krogh, "Reachability analysis of nonlinear differential-algebraic systems," *IEEE Trans. Automat. Control*, vol. 59, no. 2, pp. 371–383, Feb. 2014.
[21] Z. Xu, A. A. Julius, and J. H. Chow, "Optimal energy storage control for frequency regulation under temporal logic specifications," in *Proc. Amer. Control Conf.*, Seattle, WA, USA, May 2017, pp. 1874–1879.
[22] A. A. Julius, "Trajectory-based controller design for hybrid systems with affine continuous dynamics," in *Proc. IEEE Int. Conf. Autom. Sci. Eng.*, Aug. 2010, pp. 1007–1012.
[23] A. K. Winn and A. A. Julius, "Feedback control law generation for safety controller synthesis," in *Proc. IEEE Conf. Decision Control*, Dec. 2013, pp. 3912–3917.
[24] A. Bemporad, A. Garulli, S. Paoletti, and A. Vicino, "A bounded-error approach to piecewise affine system identification," *IEEE Trans. Autom. Control*, vol. 50, no. 10, pp. 1567–1580, Oct. 2005.
[25] G. E. Fainekos and G. J. Pappas, "Robustness of temporal logic specifications for continuous-time signals," *Theoretical Comput. Sci.*, vol. 410, no. 42, pp. 4262–4291, 2009.
[26] G. E. Fainekos and G. J. Pappas, "Robustness of temporal logic specifications," in *Proc. 1st Combined Int. Conf. Formal Approaches Softw. Testing Runtime Verification*, 2006, pp. 178–192.
[27] J. Wang and C. Chen, "Exact linearization of nonlinear differential algebraic systems," in *Proc. Int. Conf. Info-Tech Info-Net*, 2001, vol. 4, pp. 284–290.
[28] A. R. Khudair, "State linearization of multi-input nonlinear differential algebraic control systems," *Int. J. Contemp. Math. Sci.*, vol. 8, no. 11, pp. 499–509, 2013.
[29] S. Kolavennu, S. Palanki, and J. Cockburn, "Nonlinear control of nonsquare multivariable systems," *Chemical Eng. Sci.*, vol. 56, no. 6, pp. 2103–2110, 2001. [Online]. Available: http://www.sciencedirect.com/science/article/pii/S000925090000470X
[30] H. Abbas and G. Fainekos, "Computing descent direction of MTL robustness for non-linear systems," in *Proc. IEEE Amer. Control Conf.*, Jun. 2013, pp. 4405–4410.
[31] Y. Annpureddy, C. Liu, G. Fainekos, and S. Sankaranarayanan, *S-TaLiRo: A Tool for Temporal Logic Falsification for Hybrid Systems*. Berlin, Germany: Springer, 2011, pp. 254–257.
[32] K. P. Bennett and O. L. Mangasarian, "Multicategory discrimination via linear programming," *Optimization Methods Softw.*, vol. 3, pp. 27–39, 1992.
[33] Y. Susuki, T. Sakiyama, T. Ochi, T. Uemura, and T. Hikihara, "Verifying fault release control of power system via hybrid system reachability," in *Proc. 40th North Amer. Power Symp.*, Sep. 2008, pp. 1–6.

Zhe Xu (S'16) received the B.S. and M.S. degrees in electrical engineering from Tianjin University, Tianjin, China, in 2011 and 2014, respectively. He is currently working toward the Ph.D. degree in electrical engineering at the Rensselaer Polytechnic Institute, Troy, NY, USA.

His research interests include temporal logic, systems and control, hybrid systems, and power systems.

Agung Julius (M'06) received the Ph.D. degree in applied mathematics from the University of Twente, Enschede, The Netherlands, in 2005.

From 2005 to 2008, he was a Postdoctoral Researcher with the University of Pennsylvania, Philadelphia, PA, USA. Since 2008, he has been with the Department of Electrical, Computer, and Systems Engineering, Rensselaer Polytechnic Institute, Troy, NY, USA, where he is currently an Associate Professor. His research interests include systems and control, systems biology, stochastic models in systems biology, control of biological systems, hybrid systems, and mathematical systems theory.

Joe H. Chow (F'92) received the B.S. degree from the University of Minnesota, Minneapolis, MN, USA, and the M.S. and Ph.D. degrees from the University of Illinois, Urbana–Champaign, IL, USA.

After working with General Electric Power System Business, Schenectady, NY, USA, he joined the Rensselaer Polytechnic Institute in 1987, and is a Professor of electrical, computer, and systems engineering and the Campus Director of the NSF/DOE CURENT ERC. His research interests include power system dynamics and control, renewable resources, voltage stability, and synchronized phasor data.

Dr. Chow was the recipient of the Donald Eckman Award of American Automatic Control Council, the Control System Technology Award of the IEEE Control System Society, and the Charles Concordia Power System Engineering Award of the IEEE Power and Energy Society. He is a member of the National Academy of Engineering.